Macromolecules

Article

pubs.acs.org/Macromolecules

Hydrogen-Bonding-Induced Nanophase Separation in Giant Surfactants Consisting of Hydrophilic [60]Fullerene Tethered to Block Copolymers at Different Locations

Zhiwei Lin,[†] Pengtao Lu,[†] Chih-Hao Hsu,[†] Jian Sun,[†] Yangbin Zhou,[†] Mingjun Huang,[†] Kan Yue,[†] Bo Ni,[†] Xue-Hui Dong,[†] Xiaochen Li,[†] Wen-Bin Zhang,*[,†,‡] Xinfei Yu,*[,†] and Stephen Z. D. Cheng*[,†]

[†]Department of Polymer Science, College of Polymer Science and Polymer Engineering, The University of Akron, Akron, Ohio 44325-3909, United States

[‡]Key Laboratory of Polymer Chemistry & Physics of Ministry of Education, Center for Soft Matter Science and Engineering, College of Chemistry and Molecular Engineering, Peking University, Beijing 100871, P. R. China

Supporting Information

ABSTRACT: Phase behaviors of two series of giant surfactants consisting of a hydrophilic [60]fullerene (AC_{60}) molecular nanoparticle (MNP) tethered to a polystyrene-*block*-poly(ethylene oxide) (PS-*b*-PEO) block copolymer were investigated. The physical location of AC_{60} MNP was specifically designed to be at the end of the PS block (AC_{60}-PS-PEO) or at the junction point [PS-(AC_{60})-PEO] between the PS and PEO blocks. Self-assemblies of these two series of giant surfactants in the bulk revealed that the incorporation of AC_{60} MNPs leads to nanophase separation of originally disordered PS-*b*-PEO block copolymers having their block lengths shorter than the limiting value for the nanophase separation in the PS-*b*-PEO precursors. Based on small-angle X-ray scattering and transmission electron microscopy results, three ordered nanostructures were observed in these two series of giant surfactants, including lamellae, double gyroids, and cylinders, all of which possess domain sizes smaller than 10 nm. Two pairs of topological isomers, AC_{60}-PS_{50}-PEO_{45} and PS_{50}-(AC_{60})-PEO_{45} as well as AC_{60}-PS_{78}-PEO_{45} and PS_{78}-(AC_{60})-PEO_{45}, were explicitly investigated to reveal the topological effect on self-assembly behaviors of these giant surfactants. The results provided evidence of the physical location and distribution of the AC_{60} MNPs within the nanophase-separated domains and demonstrated abilities to stabilize the different structures via topological variations. This study thus affords an efficient and practical strategy for the design and preparation of giant surfactants to construct ordered nanostructures for technologically relevant applications.

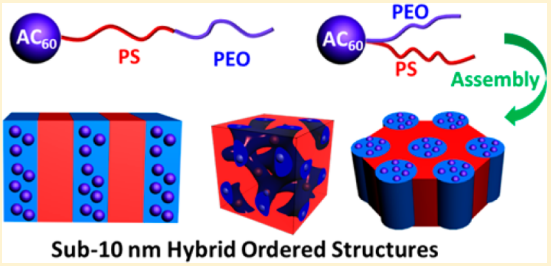

Downloaded by UNIV OF AKRON on August 28, 2015 | http://pubs.acs.org
Publication Date (Web): August 6, 2015 | doi: 10.1021/acs.macromol.5b00741

INTRODUCTION

Precise assemblies of hybrid materials containing functionalized nanoparticles (NPs) over multiple length scales have been one of the most essential themes in the fields of nanotechnology over the past two decades.[1−7] Diblock copolymers (BCPs) with immiscible blocks can form a variety of periodically ordered structures including lamellae (Lam), double gyroid (DG), hexagonally packed cylinder (Hex), and body-centered cubic sphere (BCC) phases through nanophase separation.[8−11] When physically blending NPs with BCPs, these nanophase-separated structures may serve as facile templates for controlling the NPs locations and distributions within the structures.[12−20] Alternatively, chemically tethering polymers onto NPs provides another robust approach to create hierarchical nanostructures with controlled NP composition.[21−26]

Recently, we have developed a library of new hybrid materials based on polymer-tethered molecular NPs (MNPs).[27−31] They have been regarded as giant surfactants since they capture the structural features of small-molecule surfactants yet possess much larger sizes comparable to BCPs.[27,32] It has been demonstrated that giant surfactants exhibit intriguing self-assembling behaviors in the bulk and solution states.[28,32−36] One representative example is the giant surfactant composed of a hydroxyl-group-functionalized polyhedral oligomeric silsesquioxane (POSS) tethered by a polystyrene (PS) tail. They are able to self-assemble into various nano-ordered structures in the bulk with a feature size around or below 10 nm.[28] The majority of studies so far are focusing on the giant surfactants composed of MNP(s) tethered by homopolymer(s). Incorporating BCP with heterogeneous compositions into giant surfactants are not only of scientific interest in creating new and diversified hybrid self-assembled nanostructures but also of practical importance to achieve specific and tunable properties for technological applications.[37−41]

Computer simulations have predicted rich and intriguing phase behaviors of giant surfactants composed of MNP tethered by BCP,[42−44] while experimental investigations of

Received: April 9, 2015
Revised: July 26, 2015
Published: August 6, 2015

 © 2015 American Chemical Society

DOI: 10.1021/acs.macromol.5b00741
Macromolecules 2015, 48, 5496−5503

Scheme 1. Chemical Structures and Assemblies of AC_{60}-PS_n-PEO_m and PS_n-(AC_{60})-PEO_m Giant Surfactants

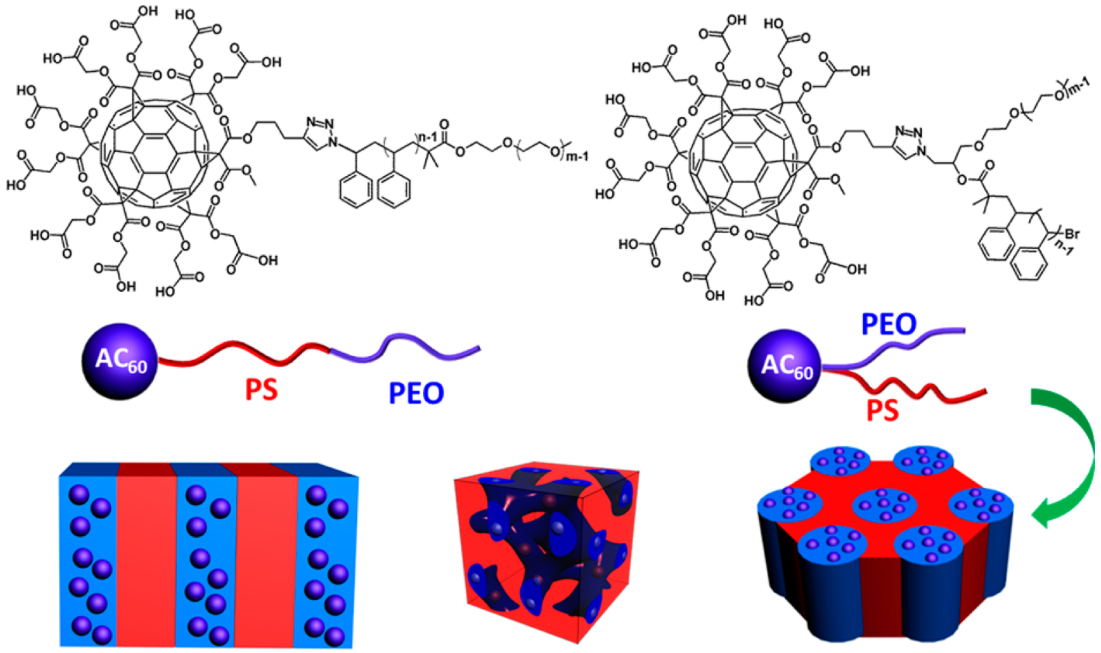

these giant surfactants are just beginning. In this article, we report our recent efforts on the design and synthesis of giant surfactants consisting of a carboxylic acid-functionalized hydrophilic [60]fullerene (AC_{60}) tethered onto a polystyrene-*block*-poly(ethylene oxide) (PS-*b*-PEO) BCP. The physical location of AC_{60} is either at the PS block end (AC_{60}-PS-PEO) or at the junction point [PS-(AC_{60})-PEO] between the PS and PEO blocks to generate two different topologies. For PEO and PS blocks, their Flory interaction parameter is χ = 0.08. This requires that a lower limit molecular mass of this BCP must exceed a threshold (in the vicinity of 16 kg/mol) in a lamellar form to reach a sufficient immiscibility (χN, N is the degree of polymerization), yet this molecular mass corresponds to a lower limiting domain size of 18−20 nm.[45−47] Since the PEO and PS block molecular masses chosen in this study are sufficiently low, the PS-*b*-PEO precursors do not exhibit nanophase separation in the melt. Nevertheless, these two series of giant surfactants possess hydrogen bonds associated with the hydrophilic AC_{60} and PEO blocks, and they drive the nanophase separation, resulting in the formation of various ordered nanostructures, as illustrated in Scheme 1. Specifically, topological isomers with identical compositions and molecular masses but different AC_{60} locations in these giant surfactants provide an opportunity to illustrate the topological effect on the nanophase-separated structures. This series of materials may thus provide a versatile and practical platform for manipulating the distribution of AC_{60} MNPs within the PEO block domains and tailoring the hybrid ordered structures with feature sizes down to sub-10 nm.

EXPERIMENTAL SECTION

Synthesis of AC_{60}-PS_n-PEO_m and PS_n-(AC_{60})-PEO_m Giant Surfactants. The syntheses of the AC_{60}-PS_n-PEO_m giant surfactants are outlined in Scheme S1. Precisely defined [5:1]-hexakis adducts of C_{60} bearing one terminal alkyne and ten protected carboxylic acid groups (TC_{60}-alkyne) and the azide-functionalized PS-*b*-PEO at the PS block end (N_3-PS_n-PEO_m) or at the junction point [PS_n-(N_3)-PEO_m] were synthesized according to the procedures reported in our previous publications.[35,48] The conjugation of TC_{60}-alkyne and N_3-PS_n-PEO_m was achieved by azide−alkyne "click" chemistry to afford TC_{60}-PS_n-PEO_m. In Fourier transform infrared spectroscopy (FTIR) experiments, the complete disappearance of absorbance band from azide group at ca. 2100 cm^{-1} gives the evidence of successful reaction between TC_{60}-alkyne and N_3-PS_n-PEO_m (Figure S1).[30,31,49] The well-defined structures of TC_{60}-PS_n-PEO_m were unambiguously characterized by nuclear magnetic resonance (NMR) spectra including ^{1}H NMR, ^{13}C NMR, and size-exclusion chromatography (SEC) experiments (see Supporting Information). In the ^{1}H NMR and ^{13}C NMR spectra, the signals of major characteristic protons and carbons attributed to the TC_{60}, PS, and PEO can be clearly observed. In the SEC profiles, the curve of TC_{60}-PS_n-PEO_m shifts to lower retention volume relative to the N_3-PS_n-PEO_m owing to the increase of molecular weight. The monomodal profile remains with narrow polydispersity ($Đ$ = 1.06), revealing the high uniformity of TC_{60}-PS_n-PEO_m. The deprotection of *tert*-butyl groups on TC_{60} was readily achieved by treating with CF_3COOH in CH_2Cl_2. The final products (AC_{60}-PS_n-PEO_m) were obtained without any further purification. The complete deprotection was evidenced by the disappearance of *tert*-butyl protons at 1.47 ppm in the ^{1}H NMR spectrum (Figure S2) and *tert*-butyl carbons at 28.1 ppm in the ^{13}C NMR spectrum (Figure S3). Following similar synthetic procedures, AC_{60} was also successfully tethered at the junction point of PS-*b*-PEO, affording the PS_n-(AC_{60})-PEO_m series (Scheme S2). Following the designed synthetic procedures in Scheme S3, AC_{60} can be tethered at the PEO block end to afford AC_{60}-PEO_m-PS_n series. The well-defined structures of as-synthesized PS_n-(AC_{60})-PEO_m and AC_{60}-PEO_m-PS_n were confirmed by the NMR, FTIR, and SEC (see Figures S5−S9).

Sample Preparations for SAXS and TEM Experiments. The freeze-dried powder samples were first thermally annealed at 120 °C under a nitrogen atmosphere for up to 12 h. The samples were then cooled to room temperature and used for SAXS measurements. Thin slices of the bulk samples with the thickness of 60−80 nm were obtained at −120 °C utilizing a Reichert Ultracut S (Leica) microtome on annealed samples embedded in epoxy monolith. The slices were carefully collected onto copper grids coated with amorphous carbon for TEM experiments. When necessary, osmium tetroxide (OsO_4) staining of the samples was performed at room temperature overnight.

Small-Angle X-ray Scattering (SAXS). SAXS patterns were collected on a Rigaku MicroMax 002+ instrument equipped with a two-dimensional (2D) multiwire area detector and a microfocus sealed copper tube. The wavelength of the X-ray is 0.154 nm, with working

Downloaded by UNIV OF AKRON on August 28, 2015 | http://pubs.acs.org
Publication Date (Web): August 6, 2015 | doi: 10.1021/acs.macromol.5b00741

DOI: 10.1021/acs.macromol.5b00741
Macromolecules 2015, 48, 5496−5503

Table 1. Summary of Characterization Data for Synthesized Giant Surfactants

sample	$M_{n,PS}$[a] (kg/mol)	$M_{n,PEO}$ (kg/mol)	V_{PS}[b]	V_{PEO}[b]	$V_{AC_{60}}$[b]	$Đ$[c]	phase structure[d]	d_1[e] (nm)
AC_{60}-PS_{28}-PEO_{45}	2.9	2.0	0.47	0.31	0.22	1.06	Lam	8.0
AC_{60}-PS_{50}-PEO_{45}	5.2	2.0	0.62	0.23	0.15	1.09	Lam	8.8
AC_{60}-PS_{52}-PEO_{45}	5.4	2.0	0.63	0.22	0.15	1.07	DG	9.2
AC_{60}-PS_{64}-PEO_{45}	6.6	2.0	0.67	0.20	0.13	1.08	Hex	9.3
AC_{60}-PS_{78}-PEO_{45}	8.1	2.0	0.71	0.17	0.12	1.07	Hex	10.0
AC_{60}-PS_{160}-PEO_{273}	16.6	12.0	0.56	0.39	0.05	1.09	Lam	17.0
PS_{50}-AC_{60}-PEO_{45}	5.2	2.0	0.62	0.23	0.15	1.08	Lam	11.4
PS_{78}-AC_{60}-PEO_{45}	8.1	2.0	0.71	0.17	0.12	1.08	Hex	12.9
AC_{60}-PEO_{45}-PS_{28}	2.9	2.0	0.47	0.31	0.22	1.09	Lam	12.6

[a]Molecular weights of the PS blocks were calculated based on NMR results. [b]Volume fractions were calculated from molecular weight and density values; see Supporting Information for detailed calculation. [c]Polydispersity of giant surfactants were obtained from SEC measurements using a PS standard calibration curve. [d]The phase structures were determined by SAXS and TEM. [e]The domain sizes were obtained based on SAXS results.

voltage and current of 45 kV and 0.88 mA, respectively. The scattering vector (q) was calibrated using silver behenate with the primary reflection peak at q = 1.067 nm^{-1}. The SAXS diffraction patterns with the q value range between 0.15 and 3.0 nm^{-1} were collected. The recording time for each data was 15 min. The data were analyzed with the Rigaku SAXSgui software.

Transmission Electron Microscopy (TEM). The bright-field (BF) TEM images of the microtomed samples were taken on a JEOL-1230 TEM equipped with a digital CCD camera and accessory digital imaging system, collecting with an accelerating voltage of 120 kV. The periodic domain sizes of ordered structures obtained from TEM images were based on an average of ten independent measurements. The calibration of the length scale on TEM images were carried out based on grating replica crossed lines.

RESULTS AND DISCUSSION

Assemblies of AC_{60}-PS_n-PEO_m Giant Surfactants in Lam Structures. Table 1 summarizes molecular characterizations of the giant surfactants studied in this work. All the synthesized giant surfactants possess narrow polydispersities ($Đ$ < 1.10) with well-defined chemical structures. Prior to thermal treatment of as-prepared samples, it is essential to examine their thermal stability. As illustrated by TGA analysis (see Figure S10), no apparent weight loss was observed at temperature lower than 200 °C at a hearing rate of 10 °C/min under a N_2 atmosphere, indicating good thermal stability of the samples below 150 °C (our thermal annealing temperature was at 120 °C).

Figure 1a shows a 1D SAXS pattern of AC_{60}-PS_{28}-PEO_{45}. There are two scattering peaks having a q-ratio of 1:2, representing a Lam structure with a periodic domain spacing of 8.0 nm (calculated via $d = 2\pi/q$, where the first-order diffraction peak is centered at q = 0.78 nm^{-1}). It should be noted that since the molecular mass of PS_{28}-b-PEO_{45} is lower than the limiting value of the nanophase separation for PS-b-PEO copolymers (~16 kg/mol),[45−47] the BCP precursor does not form a nanophase separated, ordered structure in the melt (see SAXS pattern shown in Figure S11). The formation of Lam structure is also validated in real space via a BF TEM image of the microtomed AC_{60}-PS_{28}-PEO_{45} bulk sample after OsO_4 staining as shown in Figure 1b. The alternative dark (attributed to the AC_{60} and PEO blocks) and gray (the PS blocks) domains in parallel arrangement possess an overall thickness of 8.0 ± 0.3 nm, in good agreement with the calculated value based on the SAXS result.

Figure 1c shows a BF TEM image for another AC_{60}-PS_{28}-PEO_{45} microtomed thin sample without OsO_4 staining. The dark domains with an average width of 3.5 ± 0.4 nm in this figure only represent the region where the AC_{60} MNPs are located due to its higher electron density. Compared with the stained samples with the width measured to be 4.0 ± 0.3 nm in Figure 1b, where both the AC_{60} MNPs and the PEO blocks are stained by OsO_4, this small difference indicates that the AC_{60} MNPs are distributed across the layer spacing of the AC_{60}/PEO block domain. Only the locations near the interfaces between the PEO and PS blocks may contain less AC_{60} MNPs.

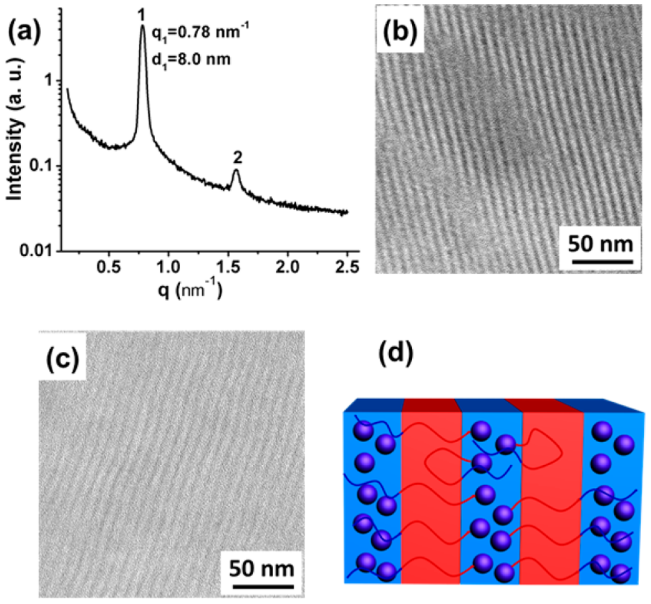

Figure 1. (a) 1D SAXS pattern and (b) BF TEM image of AC_{60}-PS_{28}-PEO_{45}. The BF TEM image is obtained after OsO_4 staining, where both AC_{60} and PEO are OsO_4-stained (dark: the AC_{60} and PEO blocks; gray: the PS blocks). (c) BF TEM image of AC_{60}-PS_{28}-PEO_{45} without staining (dark: AC_{60}; gray: PS blocks and PEO blocks). (d) Proposed lamellar model formed by AC_{60}-PS_{28}-PEO_{45} (red: the PS domains; blue: the PEO and AC_{60} mixed domains).

Both the SAXS and TEM experimental results suggest that the conjugation of the AC_{60} MNP at the PS block end of PS_{28}-b-PEO_{45} enhances the immiscibility and promotes nanophase separation. In order to illustrate that the AC_{60} MNPs are interacting with the PEO blocks via hydrogen bonding, we compared the crystallization behavior of the precursor PS_{28}-b-PEO_{45} BCP observed in differential scanning calorimetry (DSC) with that of AC_{60}-PS_{28}-PEO_{45}. Both of the samples were first cooled down from 120 to −80 °C at a cooling rate of 10 °C/min, and then the samples were heated from that

Downloaded by UNIV OF AKRON on August 28, 2015 | http://pubs.acs.org
Publication Date (Web): August 6, 2015 | doi: 10.1021/acs.macromol.5b00741

DOI: 10.1021/acs.macromol.5b00741
Macromolecules 2015, 48, 5496−5503

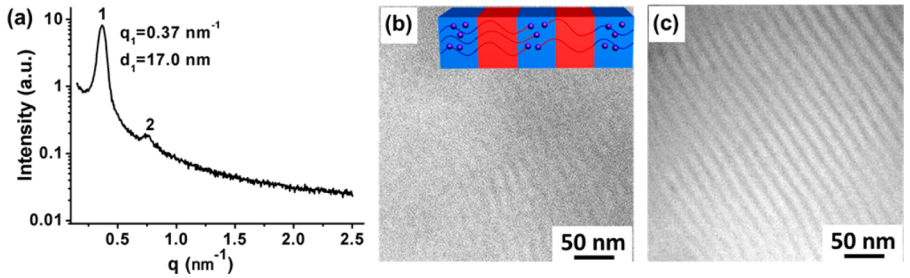

Figure 2. (a) 1D SAXS pattern of AC_{60}-PS_{160}-PEO_{273}. BF TEM images of AC_{60}-PS_{160}-PEO_{273} (b) without and (c) with OsO_4-staining. Inset is the proposed lamellar model for AC_{60}-PS_{160}-PEO_{273}.

temperature to 120 °C. Figure S12 shows that in the DSC heating thermal diagram of PS_{28}-*b*-PEO_{45} an endothermic peak of the PEO crystal melting can be observed at a temperature of ~42 °C. This indicates that PEO crystals were formed during the prior cooling process. However, the giant surfactant AC_{60}-PS_{28}-PEO_{45} does not show any thermal events in the same temperature range, revealing that the PEO blocks in AC_{60}-PS_{28}-PEO_{45} do not crystallize during the cooling process. This is indirect evidence to illustrate that the AC_{60} MNPs and PEO blocks are interacting with each other via hydrogen bonding and thus preventing crystallization of the PEO blocks in AC_{60}-PS_{28}-PEO_{45}. Direct evidence can be obtained via FTIR experiment. Figure S13 shows FTIR spectra of AC_{60}-PS_{28}-PEO_{45} before (neat dry samples once precipitating out in solution) and after thermal annealing (the nanophase separation has taken place). A new absorbance band centered at ca. 1732 cm^{-1}, corresponding to the hydrogen bonding between the carboxylic acid and PEO,[50] appears after the thermal annealing. This indicates that the hydrogen bonding has evolved between the PEO blocks and AC_{60} MNPs to result in enhancement of the segregation strength with the PS blocks. It is worth noting that no ordered structures are formed in the TC_{60}-PS_{28}-PEO_{45} precursor (the samples before deprotection of carboxylic acid groups on C_{60} and thus without hydrogen bonding) after thermal annealing, revealed by a broad scattering halo in the SAXS pattern (Figure S14). Thus, the AC_{60}/PEO block interaction facilitates the nanophase separation of AC_{60}-PS_{28}-PEO_{45}.

To further illustrate that the interaction between the AC_{60} and PEO block increases the segregation strength and compare their self-assembly behaviors, a blend of AC_{60}/PS_{28}-PEO_{45} with the molar ratio of 1:1 as well as a new giant surfactant sample, AC_{60}-PEO_{45}-PS_{28} (the AC_{60} was tethered at the PEO block end), was prepared and subjected to the identical thermal annealing procedure of AC_{60}-PS_{28}-PEO_{45}. Ordered Lam structures with *d*-spacings of 12.8 and 12.6 nm were observed in the blend and AC_{60}-PEO_{45}-PS_{28}, respectively, based on the SAXS results (Figures S15a and S16a). Although AC_{60}/PS_{28}-*b*-PEO_{45} blend, AC_{60}-PEO_{45}-PS_{28}, and AC_{60}-PS_{28}-PEO_{45} possess the exactly identical chemical composition and all of them form Lam structures, the periodic spacings of those lamellae for AC_{60}/PS_{28}-*b*-PEO_{45} blend (12.8 nm) and AC_{60}-PEO_{45}-PS_{28} (12.6 nm) are more than 55% larger than that of AC_{60}-PS_{28}-PEO_{45} (8.0 nm). To account for this difference, we argue that the hydrophilic AC_{60} MNPs are concentrated at the center of the PEO domain surrounded by the PEO blocks in the blend, as schematically shown in Figure S15b, and the PS domain is constructed by a double layer structure. The PEO blocks in the blend are also found to not crystallize (Figure S17), and this lamellar model for the blend can be proven by BF TEM images in Figures S15c and S15d (see also the discussion in the Supporting Information). This is also consistent with the previously reported simulations[51,52] and experimental observations[12,13] that NPs are favorably located at the center of compatible polymer domain to balance the loss of translational entropy of NPs and potential polymer block stretching penalties created by distributing NPs throughout the domain.[12,51] For AC_{60}-PEO_{45}-PS_{28}, a double-layer PS domain can also be expected, yet a random distribution of AC_{60} MNPs in the PEO domain can be deduced since no increase of the dark domain size after both AC_{60} MNPs and PEO were stained by OsO_4 in the BF TEM images (Figures S16c and S16d). For AC_{60}-PS_{28}-PEO_{45}, the AC_{60} MNPs are arranged throughout the PEO domain as shown in Figure 1d. Owing to the chemical linkage of AC_{60} MNPs with PS block ends, the hydrophobic PS domain within AC_{60}-PS_{28}-PEO_{45} lamellae has to be constructed by a single layer of PS blocks, as schematically shown in the Figure 1d. The single-layer arrangement of PS blocks reduces the overall *d*-spacing of the AC_{60}-PS_{28}-PEO_{45} lamellae. Therefore, the more than 55% difference in the periodic spacings between AC_{60}/PS_{28}-*b*-PEO_{45} blend, AC_{60}-PEO_{45}-PS_{28}, and AC_{60}-PS_{28}-PEO_{45} is caused by the double-layer versus the single-layer PS domains in these samples.

To confirm the proposed model in Figure 1d, PS_{160}-*b*-PEO_{273} and AC_{60}-PS_{160}-PEO_{273} with high molecular masses of both blocks were also prepared, since the PS and PEO blocks in this case possess sufficient segregation strength to generate the nanophase separation without incorporating with the AC_{60} MNPs. The SAXS and TEM results for AC_{60}-PS_{160}-PEO_{273} after the thermal annealing are shown in Figure 2, and the results of PS_{160}-*b*-PEO_{273} are shown in Figure S18. Lam structures are observed in both cases, as indicated by the two scattering peaks with a *q*-ratio of 1:2. The periodic spacing of PS_{160}-*b*-PEO_{273} is calculated to be 27.5 nm, while that of AC_{60}-PS_{160}-PEO_{273} is 17.0 nm. Again, this periodicity difference must be resulted from a single layer of the PS blocks in AC_{60}-PS_{160}-PEO_{273} versus a double layer of PS blocks in PS_{160}-*b*-PEO_{273}. Figures 2b and 2c show the BF TEM images of AC_{60}-PS_{160}-PEO_{273} without and with OsO_4 staining. Owing to the relatively low volume fraction (ca. 5%) and random distribution of AC_{60} MNPs, it is difficult to observe the continuous dark AC_{60}-concentrated domain for the nonstained sample (Figure 2b). Upon staining, the dark domain consisting of the AC_{60} MNPs and PEO can be clearly identified (Figure 2c), where the periodic spacing of lamellae is measured as 17.0 ± 1.0 nm. It is in good agreement with that obtained in Figure 2a. These results further validate that the AC_{60} MNPs distribute throughout instead of aggregate within the PEO domain.

Versatile Assemblies of AC_{60}-PS_n-PEO_m Giant Surfactants. In addition to Lam structure, DG and Hex structures are

Downloaded by UNIV OF AKRON on August 28, 2015 | http://pubs.acs.org
Publication Date (Web): August 6, 2015 | doi: 10.1021/acs.macromol.5b00741

DOI: 10.1021/acs.macromol.5b00741
Macromolecules 2015, 48, 5496−5503

readily formed in AC_{60}-PS_m-PEO_n giant surfactants by varying the PS block length. As the PS molecular mass increases to N = 52 (AC_{60}-PS_{52}-PEO_{45}), multiple scattering peaks with a q-ratio of $\sqrt{6}:\sqrt{8}:\sqrt{20}:\sqrt{22}$ are observed in the SAXS pattern (Figure 3a). The domain spacing of (211) is calculated to be

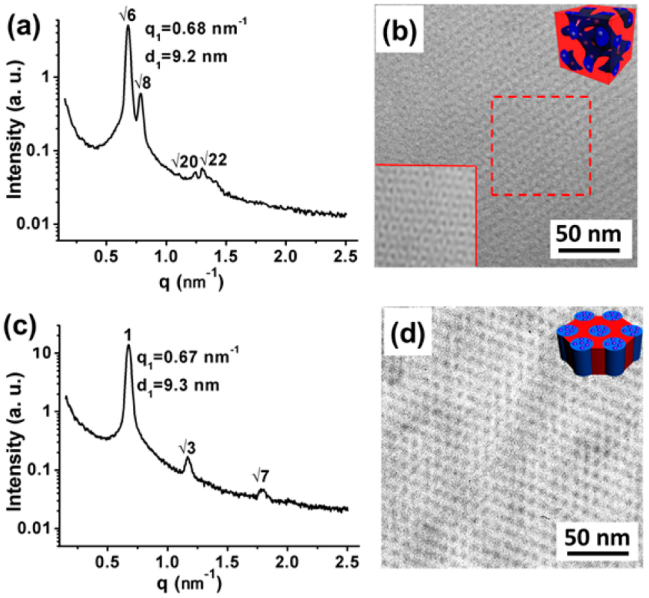

Figure 3. 1D SAXS patterns and BF TEM images of order structures of (a, b) for AC_{60}-PS_{52}-PEO_{45} and (c, d) for AC_{60}-PS_{64}-PEO_{45}. BF TEM images are obtained after both the AC_{60} and PEO are OsO_4-stained. Insets are TEM image (b, lower left) in selected area after Fourier filtering and models proposed for DG (b, upper right) and Hex (d, upper right).

9.2 nm on the basis of the first scattering peak in this figure. The BF TEM image exhibits a wheel-like pattern with the distance of 9.0 ± 0.5 nm between two neighboring wheel centers (Figure 3b and the inset). Both results clearly verify the formation of a DG structure. A Hex structure is observed as further increasing the PS block length. It is evidenced by the SAXS pattern of AC_{60}-PS_{64}-PEO_{45} in Figure 3c where a q-ratio of $1:\sqrt{3}:\sqrt{7}$ for three scattering peaks can be identified. The Hex structure is also confirmed by BF TEM image of a microtomed AC_{60}-PS_{64}-PEO_{45} thin film sample as shown in Figure 3d. The (100) d-spacing of this Hex structure is measured to be 9.5 ± 0.5 nm via the TEM observation, agreeing well with the calculated value of 9.3 nm based on the SAXS data. It can be expected that the AC_{60} MNPs are also associated with the PEO blocks and separated from the PS blocks in the DG and Hex structures because of hydrogen bonding involved between the PEO blocks and AC_{60} and low molecular masses of PS_{52}-b-PEO_{45} and PS_{64}-b-PEO_{45}. Note that without AC_{60} MNPs, these two PS-b-PEO BCPs and two additional PS_{74}-b-PEO_{114} and PS_{115}-b-PEO_{45} BCPs with larger molecular masses are in the disordered melt due to the fact that their molecular masses are still smaller than the lower limiting value (16 kg/mol) required for nanophase separation (see absences of scattering peaks in the SAXS patterns as shown in Figures S19 and S20).

With increasing the PS block length (also the volume fraction of PS, V_{PS}; see Table 1), the assembled structures of giant surfactants (AC_{60}-PS_n-PEO_m) undergo their phase transitions from Lam (V_{PS} = 0.47) to DG (V_{PS} = 0.63) and further to Hex (V_{PS} = 0.67). This phase transition is in good agreement with that predicted by the self-consistent mean-field (SCMF) theory for flexible BCP[53] and previous experimental observations for PS-b-polyisoprene (PI),[10] where the following sequence of phases is observed as varying V_{PS} (Lam: 0.34 < V_{PS} < 0.62; DG: 0.62 < V_{PS} < 0.66; Hex: 0.66 < V_{PS} < 0.77). These V_{PS} values at different phase structures also correspond well with the experimental observations of those values in PS-b-PEO diblock copolymers.[47,54−56]

Because of the weak segregation strength of BCP with low molecular masses, the preparation of ordered nanostructures with precise feature domain sizes smaller than 10 nm is generally challenging in neat BCP,[57−64] yet few reports are in BCP/NPs blend systems.[65] For the giant surfactants reported here, the dense carboxylic acid groups on the periphery of AC_{60} MNPs enable the formation of hydrogen bonds between the PEO blocks and AC_{60} MNPs and thus enhance the segregation strength to facilitate the nanophase separation of the PS-b-PEO at an overall molecular mass as low as 4.9 kg/mol. In addition, the monolayer arrangement in the PS block domain for AC_{60}-PS_n-PEO_m further decreases the domain size of self-assembled hybrid ordered structures to smaller than 10 nm (with size of 8.0 nm for Lam, 9.2 nm for DG, and 9.3 nm for Hex).

Effect of Giant Surfactant Topology on Self-Assembly. In order to exploit the effect of topology on the assemblies, two pairs of topological isomers, namely, AC_{60}-PS_{50}-PEO_{45} and PS_{50}-(AC_{60})-PEO_{45} as well as AC_{60}-PS_{78}-PEO_{45} and PS_{78}-(AC_{60})-PEO_{45}, were specifically prepared. Each pair of topological isomers possesses identical molecular masses of the PEO and PS blocks, but the AC_{60} MNP is attached at different physical locations (at the PS block end or at the junction point between the PEO and PS blocks). As shown in Figures 4a and 4b, both AC_{60}-PS_{50}-PEO_{45} and PS_{50}-(AC_{60})-PEO_{45} possess Lam structures, but with different periodic domain spacings (8.8 nm versus 11.4 nm). This difference can only be attributed to the tethering locations of AC_{60} MNPs (and thus the giant surfactant topology). The packing model of

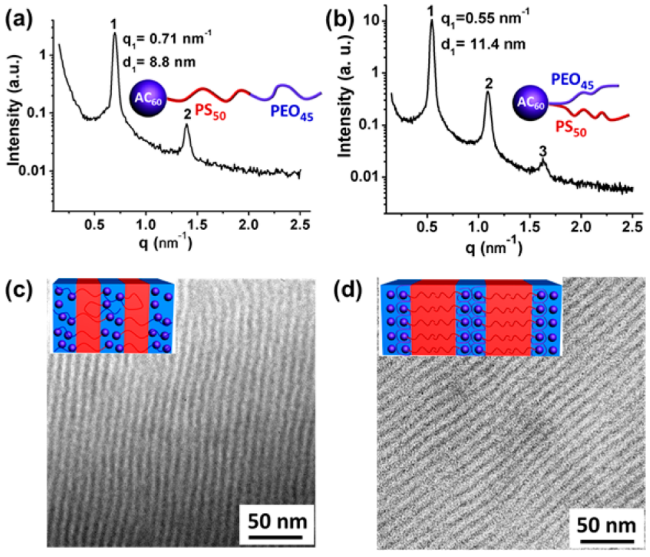

Figure 4. 1D SAXS patterns and BF TEM images of Lam structures of (a, c) for AC_{60}-PS_{50}-PEO_{45} and (b, d) for PS_{50}-(AC_{60})-PEO_{45}. Insets are the models proposed for AC_{60}-PS_{50}-PEO_{45} and PS_{50}-(AC_{60})-PEO_{45}. TEM images are obtained after staining by OsO_4, where both AC_{60} and PEO are stained.

Downloaded by UNIV OF AKRON on August 28, 2015 | http://pubs.acs.org
Publication Date (Web): August 6, 2015 | doi: 10.1021/acs.macromol.5b00741

DOI: 10.1021/acs.macromol.5b00741
Macromolecules 2015, 48, 5496−5503

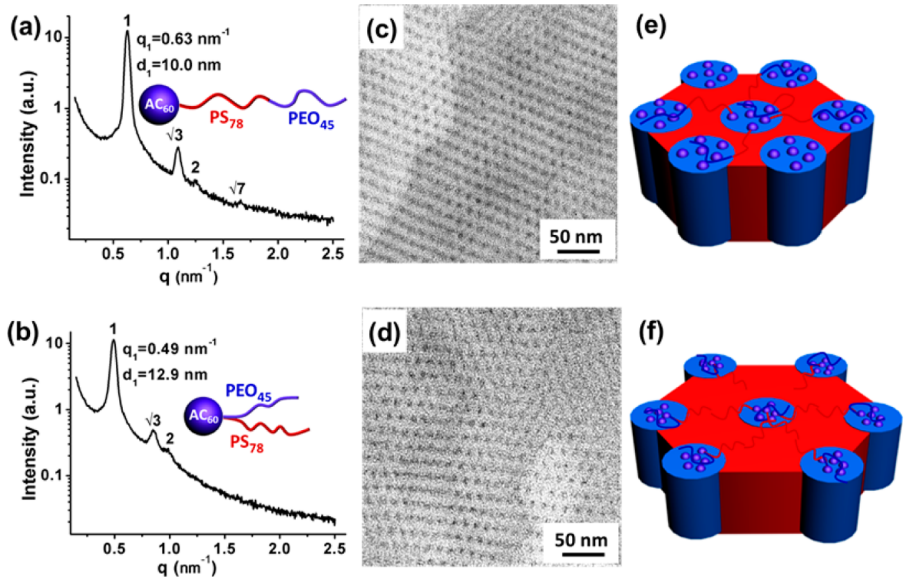

Figure 5. 1D SAXS patterns, BF TEM images and proposed models of Hex structures: (a, c, e) for AC_{60}-PS_{78}-PEO_{45}; (b, d, f) for PS_{78}-(AC_{60})-PEO_{45}.

AC_{60}-PS_{50}-PEO_{45} is shown in Figure 1d (also inserted in Figure 4c). For PS_{50}-(AC_{60})-PEO_{45}, it is suggested that its packing model possesses a double layer of the PS blocks as shown in the inset of Figure 4d. The BF TEM images of microtomed samples of AC_{60}-PS_{50}-PEO_{45} and PS_{50}-(AC_{60})-PEO_{45} after OsO_4-staining are shown in Figures 4c and 4d. The widths of gray PS domains in AC_{60}-PS_{50}-PEO_{45} and PS_{50}-(AC_{60})-PEO_{45} are measured to be 5.0 ± 0.5 and 7.0 ± 0.6 nm, respectively. The size difference of ~2 nm between these two PS domains is consistent with the results obtained in SAXS experiments (2.6 nm).

Given the identical PS block lengths in these two topological isomers, one may ask why the PS domain spacing of PS_{50}-(AC_{60})-PEO_{45} (double layer, 7 nm) is only about 40% larger but less than twice of the size compared with that of AC_{60}-PS_{50}-PEO_{45} (single layer, 5 nm). To address this issue, we calculate the stretching ratio (S) of the PS chains in the Lam, which can be characterized by

$$S = L/2R_g \quad (1)$$

where L is obtained from the PS domain spacing in the single layer model (AC_{60}-PS_{50}-PEO_{45}) or one-half of the PS domain spacing in the double-layer model [PS_{50}-(AC_{60})-PEO_{45}]. R_g is the radius of gyration of PS chain that can be calculated by

$$R_g = (N_{PS}/6)^{1/2}b \quad (2)$$

where N_{PS} is the degree of polymerization of PS and b is the average statistical segment length of PS (b = 0.68 nm).[66] The values of S for both the PS blocks in AC_{60}-PS_{50}-PEO_{45} and PS_{50}-(AC_{60})-PEO_{45} are calculated to be 1.28 and 0.90, respectively. This reveals that the PS blocks in AC_{60}-PS_{50}-PEO_{45} are relatively stretched, while those in PS_{50}-(AC_{60})-PEO_{45} are more relaxed. This may be associated with the fact that the PS blocks have no free chain ends in AC_{60}-PS_{50}-PEO_{45}, in contrast to one free chain end of the PS blocks in PS_{50}-(AC_{60})-PEO_{45}.

Another set of topological isomers, AC_{60}-PS_{78}-PEO_{45} and PS_{78}-(AC_{60})-PEO_{45}, exhibit Hex structures with different periodic spacing (d_{100}) based on the SAXS patterns in Figures 5a and 5b. They are 10.0 and 12.9 nm, respectively. The center distances between two neighboring columns (d) in these two Hex structures are thus calculated to be 11.5 and 14.9 nm ($d = 2d_{100}/\sqrt{3}$), respectively. This difference can be confirmed by the results of BF TEM images in Figures 5c and 5d, where the d values of two Hex structures are measured as 12.0 ± 0.8 and 15.0 ± 0.9 nm, respectively. The difference in the d values for these two Hex structures can also be ascribed to the distinct PS conformations. As illustrated in the Figure 5e, in the Hex of AC_{60}-PS_{78}-PEO_{45}, the PEO and AC_{60} of each giant surfactant are located either in two neighboring columns or in the same column with a PS block that is folded back. In the Hex structure of PS_{78}-(AC_{60})-PEO_{45} (Figure 5f), the PEO and AC_{60} of each molecule are expected to be located in the same column, where the PS blocks arrange in the domain with a free chain end. The latter PS conformations are more likely to increase the distance between two neighboring columns. This may associate with the fact that the PS blocks with a free chain end in PS_{78}-(AC_{60})-PEO_{45} construct the PS domains via both the tethered PS chains from neighboring columns, while in AC_{60}-PS_{78}-PEO_{45} the PS domain is formed by one PS block connected to two neighboring columns.

CONCLUSION

In summary, two series of giant surfactants with a AC_{60} MNP tethered onto a PS-*b*-PEO block copolymer either at the PS block end (AC_{60}-PS_m-PEO_n) or at the junction point [PS_m-(AC_{60})-PEO_n] of the block copolymers were designed and synthesized via "click" chemistry. Investigation of the assembly of these two series of giant surfactants reveals that the hydrogen bonding between the AC_{60} MNPs and the PEO blocks plays an essential role in facilitating the nanophase separation of originally disordered PS-*b*-PEO block copolymers and thus affording the formation of various ordered nanostructures in the bulk, such as Lam, DG, and Hex phases. In these ordered structures, the AC_{60} MNPs and PEO blocks are associated with each other in one domain and the PS blocks segregate into another. With a systematic study of their phase behaviors, we can conclude that (1) comparison between the giant surfactant

Downloaded by UNIV OF AKRON on August 28, 2015 | http://pubs.acs.org
Publication Date (Web): August 6, 2015 | doi: 10.1021/acs.macromol.5b00741

DOI: 10.1021/acs.macromol.5b00741
Macromolecules 2015, 48, 5496−5503

having MNP tethered block copolymer system with a system of mixing MNPs into block copolymers shows more controlled nanophase separations could be achieved with a smaller domain size; (2) comparison of two pairs of topological isomers, AC_{60}-PS_{50}-PEO_{45} and PS_{50}-(AC_{60})-PEO_{45}, as well as AC_{60}-PS_{78}-PEO_{45} and PS_{78}-(AC_{60})-PEO_{45} reveals that their Lam and Hex structures with different domain sizes result from the distinct PS block arrangements and their conformations in the domains; and (3) this work introduces a practical approach to the design and fabrication of hierarchical nanostructures with sub-10 nm length scales.

■ ASSOCIATED CONTENT

Supporting Information

The Supporting Information is available free of charge on the ACS Publications website at DOI: 10.1021/acs.macromol.5b00741.

Additional experimental descriptions, chemical characterization of prepared giant surfactants, supplemental discussion, and Figures S1−S20 (PDF)

■ AUTHOR INFORMATION

Corresponding Authors

*E-mail: wenbin@pku.edu.cn (W.-B.Z.).
*E-mail: xy5@zips.uakron.edu (X.Y.).
*E-mail: scheng@uakron.edu (S.Z.D.C.).

Notes

The authors declare no competing financial interest.

■ ACKNOWLEDGMENTS

We acknowledge support from the National Science Foundation (DMR-1408872). We thank Dr. Jinlin He from Soochow University for providing the samples of PS-OH.

■ REFERENCES

(1) Boal, A. K.; Ilhan, F.; DeRouchey, J. E.; Thurn-Albrecht, T.; Russell, T. P.; Rotello, V. M. *Nature* **2000**, *404*, 746−748.
(2) Glotzer, S. C.; Solomon, M. J. *Nat. Mater.* **2007**, *6*, 557−562.
(3) Whitesides, G. M.; Grzybowski, B. *Science* **2002**, *295*, 2418−2421.
(4) Haryono, A.; Binder, W. H. *Small* **2006**, *2*, 600−611.
(5) Sudeep, P. K.; Emrick, T. *ACS Nano* **2009**, *3*, 2870−2875.
(6) Huang, M.; Hsu, C.-H.; Wang, J.; Mei, S.; Dong, X.; Li, Y.; Li, M.; Liu, H.; Zhang, W.; Aida, T.; Zhang, W.-B.; Yue, K.; Cheng, S. Z. D. *Science* **2015**, *348*, 424−428.
(7) Liu, H.; Hsu, C.-H.; Lin, Z.; Shan, W.; Wang, J.; Jiang, J.; Huang, M.; Lotz, B.; Yu, X.; Zhang, W.-B.; Yue, K.; Cheng, S. Z. D. *J. Am. Chem. Soc.* **2014**, *136*, 10691−10699.
(8) Almdal, K.; Koppi, K. A.; Bates, F. S.; Mortensen, K. *Macromolecules* **1992**, *25*, 1743−1751.
(9) Bates, F. S. *Science* **1991**, *251*, 898−905.
(10) Bates, F. S.; Fredrickson, G. H. *Annu. Rev. Phys. Chem.* **1990**, *41*, 525−557.
(11) Leibler, L. *Macromolecules* **1980**, *13*, 1602−1617.
(12) Chiu, J. J.; Kim, B. J.; Kramer, E. J.; Pine, D. J. *J. Am. Chem. Soc.* **2005**, *127*, 5036−5037.
(13) Zhao, Y.; Thorkelsson, K.; Mastroianni, A. J.; Schilling, T.; Luther, J. M.; Rancatore, B. J.; Matsunaga, K.; Jinnai, H.; Wu, Y.; Poulsen, D.; Frechet, J. M. J.; Alivisatos, A. P.; Xu, T. *Nat. Mater.* **2009**, *8*, 979−985.
(14) Lin, Y.; Boker, A.; He, J.; Sill, K.; Xiang, H. Q.; Abetz, C.; Li, X.; Wang, J.; Emrick, T.; Long, S.; Wang, Q.; Balazs, A.; Russell, T. P. *Nature* **2005**, *434*, 55−59.
(15) Li, Q.; He, J.; Glogowski, E.; Li, X.; Wang, J.; Emrick, T.; Russell, T. P. *Adv. Mater.* **2008**, *20*, 1462−1466.
(16) Kim, B. J.; Chiu, J. J.; Yi, G.-R.; Pine, D. J.; Kramer, E. J. *Adv. Mater.* **2005**, *17*, 2618−2622.
(17) Bockstaller, M. R.; Lapetnikov, Y.; Margel, S.; Thomas, E. L. *J. Am. Chem. Soc.* **2003**, *125*, 5276−5277.
(18) Lee, J.-Y.; Thompson, R. B.; Jasnow, D.; Balazs, A. C. *Phys. Rev. Lett.* **2002**, *89*, 155503.
(19) Jang, S. G.; Kramer, E. J.; Hawker, C. J. *J. Am. Chem. Soc.* **2011**, *133*, 16986−16996.
(20) Warren, S. C.; Messina, L. C.; Slaughter, L. S.; Kamperman, M.; Zhou, Q.; Gruner, S. M.; DiSalvo, F. J.; Wiesner, U. *Science* **2008**, *320*, 1748−1752.
(21) Yockell-Lelièvre, H.; Desbiens, J.; Ritcey, A. M. *Langmuir* **2007**, *23*, 2843−2850.
(22) Horsch, M. A.; Zhang, Z. L.; Glotzer, S. C. *Phys. Rev. Lett.* **2005**, *95*, 056105.
(23) Pyun, J.; Matyjaszewski, K.; Kowalewski, T.; Savin, D.; Patterson, G.; Kickelbick, G.; Huesing, N. *J. Am. Chem. Soc.* **2001**, *123*, 9445−9446.
(24) Martin, T. B.; Seifpour, A.; Jayaraman, A. *Soft Matter* **2011**, *7*, 5952−5964.
(25) Akcora, P.; Liu, H.; Kumar, S. K.; Moll, J.; Li, Y.; Benicewicz, B. C.; Schadler, L. S.; Acehan, D.; Panagiotopoulos, A. Z.; Pryamitsyn, V.; Ganesan, V.; Ilavsky, J.; Thiyagarajan, P.; Colby, R. H.; Douglas, J. F. *Nat. Mater.* **2009**, *8*, 354−359.
(26) Keng, P. Y.; Shim, I.; Korth, B. D.; Douglas, J. F.; Pyun, J. *ACS Nano* **2007**, *1*, 279−292.
(27) Zhang, W.-B.; Yu, X.; Wang, C.-L.; Sun, H.-J.; Hsieh, I.-F.; Li, Y.; Dong, X.-H.; Yue, K.; Van Horn, R.; Cheng, S. Z. D. *Macromolecules* **2014**, *47*, 1221−1239.
(28) Yu, X.; Yue, K.; Hsieh, I.-F.; Li, Y.; Dong, X.-H.; Liu, C.; Xin, Y.; Wang, H.-F.; Shi, A.-C.; Newkome, G. R.; Ho, R.-M.; Chen, E.-Q.; Zhang, W.-B.; Cheng, S. Z. D. *Proc. Natl. Acad. Sci. U. S. A.* **2013**, *110*, 10078−10083.
(29) Yu, X.; Zhong, S.; Li, X.; Tu, Y.; Yang, S.; Van Horn, R. M.; Ni, C.; Pochan, D. J.; Quirk, R. P.; Wesdemiotis, C.; Zhang, W.-B.; Cheng, S. Z. D. *J. Am. Chem. Soc.* **2010**, *132*, 16741−16744.
(30) Yue, K.; Liu, C.; Guo, K.; Yu, X.; Huang, M.; Li, Y.; Wesdemiotis, C.; Cheng, S. Z. D.; Zhang, W.-B. *Macromolecules* **2012**, *45*, 8126−8134.
(31) Lin, Z.; Lu, P.; Yu, X.; Zhang, W.-B.; Huang, M.; Wu, K.; Guo, K.; Wesdemiotis, C.; Zhu, X.; Zhang, Z.; Yue, K.; Cheng, S. Z. D. *Macromolecules* **2014**, *47*, 4160−4168.
(32) Yu, X.; Li, Y.; Dong, X.-H.; Yue, K.; Lin, Z.; Feng, X.; Huang, M.; Zhang, W.-B.; Cheng, S. Z. D. *J. Polym. Sci., Part B: Polym. Phys.* **2014**, *52*, 1309−1325.
(33) Wang, Z.; Li, Y.; Dong, X.-H.; Yu, X.; Guo, K.; Su, H.; Yue, K.; Wesdemiotis, C.; Cheng, S. Z. D.; Zhang, W.-B. *Chem. Sci.* **2013**, *4*, 1345−1352.
(34) Wu, K.; Huang, M. J.; Yue, K.; Liu, C.; Lin, Z. W.; Liu, H.; Zhang, W.; Hsu, C. H.; Shi, A. C.; Zhang, W. B.; Cheng, S. Z. D. *Macromolecules* **2014**, *47*, 4622−4633.
(35) Yu, X.; Zhang, W.-B.; Yue, K.; Li, X.; Liu, H.; Xin, Y.; Wang, C.-L.; Wesdemiotis, C.; Cheng, S. Z. D. *J. Am. Chem. Soc.* **2012**, *134*, 7780−7787.
(36) Ni, B.; Huang, M.; Chen, Z.; Chen, Y.; Hsu, C.-H.; Li, Y.; Pochan, D.; Zhang, W.-B.; Cheng, S. Z. D.; Dong, X.-H. *J. Am. Chem. Soc.* **2015**, *137*, 1392−1395.
(37) Aldaye, F. A.; Palmer, A. L.; Sleiman, H. F. *Science* **2008**, *321*, 1795−1799.
(38) Balazs, A. C.; Emrick, T.; Russell, T. P. *Science* **2006**, *314*, 1107−1110.
(39) Huynh, W. U.; Dittmer, J. J.; Alivisatos, A. P. *Science* **2002**, *295*, 2425−2427.
(40) Bockstaller, M. R.; Mickiewicz, R. A.; Thomas, E. L. *Adv. Mater.* **2005**, *17*, 1331−1349.
(41) Shenhar, R.; Norsten, T. B.; Rotello, V. M. *Adv. Mater.* **2005**, *17*, 657−669.

Downloaded by UNIV OF AKRON on August 28, 2015 | http://pubs.acs.org
Publication Date (Web): August 6, 2015 | doi: 10.1021/acs.macromol.5b00741

DOI: 10.1021/acs.macromol.5b00741
Macromolecules 2015, 48, 5496−5503

(42) Glotzer, S. C.; Horsch, M. A.; Iacovella, C. R.; Zhang, Z. L.; Chan, E. R.; Zhang, X. *Curr. Opin. Colloid Interface Sci.* **2005**, *10*, 287−295.
(43) Zhu, X.; Wang, L.; Lin, J.; Zhang, L. *ACS Nano* **2010**, *4*, 4979−4988.
(44) Ma, S.; Qi, D.; Xiao, M.; Wang, R. *Soft Matter* **2014**, *10*, 9090−9097.
(45) Zhu, L.; Chen, Y.; Zhang, A.; Calhoun, B. H.; Chun, M.; Quirk, R. P.; Cheng, S. Z. D.; Hsiao, B. S.; Yeh, F.; Hashimoto, T. *Phys. Rev. B: Condens. Matter Mater. Phys.* **1999**, *60*, 10022−10031.
(46) Dong, X.-H.; Lu, X.; Ni, B.; Chen, Z.; Yue, K.; Li, Y.; Rong, L.; Koga, T.; Hsiao, B. S.; Newkome, G. R.; Shi, A.-C.; Zhang, W.-B.; Cheng, S. Z. D. *Soft Matter* **2014**, *10*, 3200−3208.
(47) Zhu, L.; Cheng, S. Z. D.; Calhoun, B. H.; Ge, Q.; Quirk, R. P.; Thomas, E. L.; Hsiao, B. S.; Yeh, F.; Lotz, B. *Polymer* **2001**, *42*, 5829−5839.
(48) Ni, B.; Dong, X.-H.; Chen, Z.; Lin, Z.; Li, Y.; Huang, M.; Fu, Q.; Cheng, S. Z. D.; Zhang, W.-B. *Polym. Chem.* **2014**, *5*, 3588−3597.
(49) Zhang, W.-B.; Tu, Y.; Ranjan, R.; Van Horn, R. M.; Leng, S.; Wang, J.; Polce, M. J.; Wesdemiotis, C.; Quirk, R. P.; Newkome, G. R.; Cheng, S. Z. D. *Macromolecules* **2008**, *41*, 515−517.
(50) Yao, L.; Watkins, J. J. *ACS Nano* **2013**, *7*, 1513−1523.
(51) Thompson, R. B.; Ginzburg, V. V.; Matsen, M. W.; Balazs, A. C. *Science* **2001**, *292*, 2469−2472.
(52) Thompson, R. B.; Ginzburg, V. V.; Matsen, M. W.; Balazs, A. C. *Macromolecules* **2002**, *35*, 1060−1071.
(53) Matsen, M. W.; Bates, F. S. *Macromolecules* **1996**, *29*, 1091−1098.
(54) Huang, P.; Zhu, L.; Cheng, S. Z. D.; Ge, Q.; Quirk, R. P.; Thomas, E. L.; Lotz, B.; Hsiao, B. S.; Liu, L.; Yeh, F. *Macromolecules* **2001**, *34*, 6649−6657.
(55) Zhu, L.; Cheng, S. Z. D.; Calhoun, B. H.; Ge, Q.; Quirk, R. P.; Thomas, E. L.; Hsiao, B. S.; Yeh, F.; Lotz, B. *J. Am. Chem. Soc.* **2000**, *122*, 5957−5967.
(56) Zhu, L.; Huang, P.; Chen, W. Y.; Ge, Q.; Quirk, R. P.; Cheng, S. Z. D.; Thomas, E. L.; Lotz, B.; Hsiao, B. S.; Yeh, F. J.; Liu, L. *Macromolecules* **2002**, *35*, 3553−3562.
(57) Son, J. G.; Hannon, A. F.; Gotrik, K. W.; Alexander-Katz, A.; Ross, C. A. *Adv. Mater.* **2011**, *23*, 634−639.
(58) Cushen, J. D.; Bates, C. M.; Rausch, E. L.; Dean, L. M.; Zhou, S. X.; Willson, C. G.; Ellison, C. J. *Macromolecules* **2012**, *45*, 8722−8728.
(59) Son, J. G.; Chang, J. B.; Berggren, K. K.; Ross, C. A. *Nano Lett.* **2011**, *11*, 5079−5084.
(60) Park, S.; Lee, D. H.; Xu, J.; Kim, B.; Hong, S. W.; Jeong, U.; Xu, T.; Russell, T. P. *Science* **2009**, *323*, 1030−1033.
(61) Bates, C. M.; Seshimo, T.; Maher, M. J.; Durand, W. J.; Cushen, J. D.; Dean, L. M.; Blachut, G.; Ellison, C. J.; Willson, C. G. *Science* **2012**, *338*, 775−779.
(62) Chang, J. B.; Son, J. G.; Hannon, A. F.; Alexander-Katz, A.; Ross, C. A.; Berggren, K. K. *ACS Nano* **2012**, *6*, 2071−2077.
(63) Isono, T.; Otsuka, I.; Kondo, Y.; Halila, S.; Fort, S.; Rochas, C.; Satoh, T.; Borsali, R.; Kakuchi, T. *Macromolecules* **2013**, *46*, 1461−1469.
(64) Cushen, J. D.; Otsuka, I.; Bates, C. M.; Halila, S.; Fort, S.; Rochas, C.; Easley, J. A.; Rausch, E. L.; Thio, A.; Borsali, R.; Willson, C. G.; Ellison, C. J. *ACS Nano* **2012**, *6*, 3424−3433.
(65) Lin, Y.; Daga, V. K.; Anderson, E. R.; Gido, S. P.; Watkins, J. J. *J. Am. Chem. Soc.* **2011**, *133*, 6513−6516.
(66) Tanaka, K.; Yoon, J. S.; Takahara, A.; Kajiyama, T. *Macromolecules* **1995**, *28*, 934−938.

Downloaded by UNIV OF AKRON on August 28, 2015 | http://pubs.acs.org
Publication Date (Web): August 6, 2015 | doi: 10.1021/acs.macromol.5b00741

DOI: 10.1021/acs.macromol.5b00741
Macromolecules 2015, 48, 5496−5503